Four-quasiparticle alignments in ^{66}Ge

E. A. Stefanova,[1,*] I. Stefanescu,[2] G. de Angelis,[3] D. Curien,[4] J. Eberth,[2] E. Farnea,[5] A. Gadea,[3] G. Gersch,[2] A. Jungclaus,[1,6] K. P. Lieb,[1] T. Martinez,[3] R. Schwengner,[7] T. Steinhardt,[2] O. Thelen,[2] D. Weisshaar,[2] and R. Wyss[8]

[1]*II. Physikalisches Institut, Universität Göttingen, D-37073 Göttingen, Germany*

[2]*Institut für Kernphysik, Universität zu Köln, D-50937 Köln, Germany*

[3]*INFN, Laboratori Nazionali di Legnaro, I-35020 Legnaro, Italy*

[4]*Institut de Recherches Subatomiques, CNRS-IN2P3, F-67037 Strasbourg, France*

[5]*INFNE, Sezione di Padova, Padova, Italy*

[6]*Instituto de Estructura de la Materia, Consejo Superior de Investigaciones Cientificas, E-28006 Madrid and Departamento de Fisica Teórica, Universidad Autónoma de Madrid, E-28049 Madrid, Spain*

[7]*Institut für Kern und Hadronenphysik, FZ Rossendorf, D-01314 Dresden, Germany*

[8]*Department of Physics, Royal Institute of Technology, 10405 Stockholm, Sweden*

(Received 16 January 2003; published 30 May 2003)

The neutron-deficient nucleus ^{66}Ge was populated at high spin in two experiments using the reaction ^{40}Ca(^{32}S,$\alpha 2p$) at beam energies of 105 and 95 MeV. In the first experiment, a self-supporting ^{40}Ca target was used, while a gold-backed target of similar thickness was used in the second experiment. γ rays were detected with the EUROBALL array, combined with the charged-particle detector array EUCLIDES and the Neutron Wall. The level scheme of ^{66}Ge was extended up to $E \approx 18$ MeV and $I^{\pi}=(23^{-})$. Above angular momentum 10^{+}, we found two sequences, connected by energetically staggered $\Delta I=1$ $M1$ transitions. The total Routhian surface calculations describe ^{66}Ge at lower spins as a γ-soft nucleus having a moderate deformation of $\beta_2 \approx 0.23$, while a triaxial deformation is predicted for the band structures above $I^{\pi}=10^{+}$. To our knowledge, this is the first observation of staggered $M1$ transitions in a deformed four-quasiparticle $\pi(g_{9/2}^2)\nu(g_{9/2}^2)$ structure.

DOI: 10.1103/PhysRevC.67.054319 PACS number(s): 23.20.Lv, 21.10.Re, 25.70.Hi, 27.50.+e

I. INTRODUCTION

The $^{66}_{32}Ge_{34}$ nucleus studied here lies close to the $N=Z$ line, between the doubly magic $^{56}_{28}Ni_{28}$ and strongly deformed neutron-deficient $^{76}_{38}Sr_{38}$ isotopes. The position between these two limits causes a complicated interplay between noncollective and collective degrees of freedom. The coexistence of prolate and oblate shapes is a typical phenomenon for the nuclei with $N,Z=34-36$, where large gaps between single-particle energies at prolate and oblate deformations were calculated [1,2]. An oblate shape was predicted for the ground-state band of ^{68}Ge by excited VAMPIR calculations [3–5]. Calculations using the IBM-3 approach [6] describe ^{66}Ge and ^{68}Ge as vibrational nuclei, while the $N=Z$ ^{64}Ge was calculated to be extremely soft towards triaxial deformation [6–8]. The question of possible γ softness in ^{66}Ge has not been discussed yet, neither have any positive-parity band structures been investigated above the first band crossing up to now. In nuclei near the $N=Z$ line, the four-quasiparticle alignment follows immediately or even overlaps with the two-quasiparticle alignment, because the neutrons and protons occupy the same orbitals and strong mixing occurs. Although in most nuclei in the $N,Z=30-42$ region the four-quasiparticle proton-neutron $g_{9/2}$ alignment is found to drive the shape to smaller deformations, triaxial Routhian surface calculations for ^{64}Ge predict a well-deformed minimum at $\beta_2 \approx 0.3$ and $\gamma \approx 15°$ [7]. The deformation-driving forces of aligned pairs of protons and neutrons were proposed (see Ref. [7] and references therein) to be due to the particle character of the $g_{9/2}$ subshell, which is above the Fermi level at $N=Z=32$. The aim of the present work was to investigate the band structures arising from the $(\pi g_{9/2}^2 \nu g_{9/2}^2)$ four-quasiparticle alignment in ^{66}Ge.

The yrast structure of ^{66}Ge was previously studied by several groups [9–13]. In the present work, we extended the level scheme by two new positive-parity and negative-parity bandlike sequences. The previously known part of the level scheme [13] was considerably complemented. Based on DCO (directional correlations of oriented states) ratio analyses, we assigned spins to most of the observed levels. To interpret the high-spin structure of ^{66}Ge, total Routhian surface calculations were performed.

II. EXPERIMENTAL METHODS AND RESULTS

A. Reaction and sorting procedure

The nucleus ^{66}Ge was populated at high spin using the reaction ^{40}Ca(^{32}S,$\alpha 2p$) at a beam energy of 105 MeV. The ^{32}S beam was delivered by the VIVITRON accelerator of the IReS in Strasburg. The target consisted of a 860 μg/cm^2 self-supporting foil of enriched ^{40}Ca. After this experiment, a second experiment was performed using the same reaction at a beam energy of 95 MeV. Here, the target consisted of 1 mg/cm^2 ^{40}Ca enriched to 99.9% and evaporated onto a 15 mg/cm^2 gold backing. In both experiments, γ rays were

*Permanent address: Institute for Nuclear Research and Nuclear Energy, BAS, 1784 Sofia, Bulgaria.

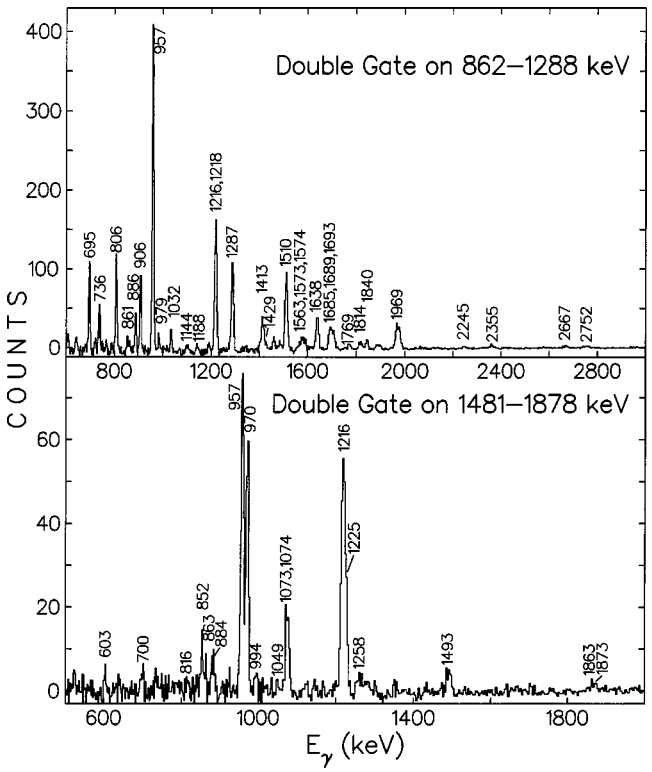

FIG. 1. Examples of doubly gated coincidence spectra, extracted from the α-γ-γ cube. Peaks labeled with their energies in keV are assigned to ^{66}Ge.

detected with the EUROBALL array [14], consisting of 15 cluster and 26 clover Ge detectors. Charged particles were detected with the 4π EUCLIDES array [15], consisting of 40 silicon $\Delta E-E$ telescopes. Neutrons were identified with the neutron wall [16], built up of 50 liquid-scintillator neutron detectors arranged to cover the forward 1π part of EUROBALL. The trigger conditions for collecting events in the various evaporation channels were set to either at least two Ge detectors (clover or cluster segments) and one neutron identified in the neutron wall fired in coincidence or when at least three Ge detectors and one event (neutron or γ) in a neutron detector were registered in coincidence. E_γ-E_γ matrices gated on the number of protons, neutrons, and α particles, corresponding to different reaction channels were sorted off-line for all detector combinations. An add-back correction for Compton scattering was performed. Doppler-shift correction for a constant recoil velocity of $v/c=2.6\%$ was made when sorting the data from the self-supporting-target experiment. E_γ-E_γ-E_γ cubes with and without gates on $1p$, $1n$, and 1α were sorted.

In the present experiment, ^{66}Ge was populated via the $2p1\alpha$ reaction channel. The level scheme of ^{66}Ge was constructed on the basis of the analysis of doubly gated spectra extracted from the cube gated on an α particle, using the code LEVIT8R [17]. Examples of doubly gated coincidence spectra, revealing the newly observed transitions in ^{66}Ge are shown in Fig. 1. The γ rays assigned to ^{66}Ge on the basis of the present experiment are listed in Table I[34]. The first column gives the energies of the γ rays belonging to ^{66}Ge, obtained from the $2p1\alpha$-gated matrix, containing data from the backed-target experiment. These energies are presented in the level scheme shown in Fig. 2. In the second and third columns the energies and relative intensities of the observed transitions in ^{66}Ge derived from a coincidence spectrum gated on the ground-state transition are given. This spectrum was extracted from a matrix gated on $2p1\alpha$ events, sorted from coincidence data with the self-supporting target. From a comparison of the energies derived from the two experiments, one can see that the results agree in most cases, and the maximum deviation is approximately 2.5 keV. Note that the linewidth for a transition of about 1 MeV was approximately 16 keV in the experiment with the self-supporting target, due to Doppler broadening.

B. Angular correlations of γ rays

Directional correlations of coincident γ rays from oriented states were used to deduce multipole orders of the transitions and, thus, to assign spins to the levels. A detailed description of this method can be found in Refs. [18–20]. Because of their composite structure, the EUROBALL detectors form 13 rings positioned at angles of about 72°, 81°, 99°, 108°, 123°, 129°, 133°, 137°, 141°, 146°, 149°, 156°, and 163° to the beam. To deduce the DCO ratios, coincidences corresponding to all possible two-ring combinations formed from the rings at angles of 72°, 81°, 99°, 108° and the rings at 146°, 149°, 156°, 163° were sorted. Then, these matrices were added up in such a way that the γ rays detected at angles around 90° were on the first axis, and those detected at angles around 155° were on the second axis. We used the equation $R_{DCO}=\epsilon_{\gamma_1}(150°)\,\epsilon_{\gamma_2}(90°)\,\mathrm{I}_{\gamma_2}(GATE^{150°}_{\gamma_1})/\epsilon_{\gamma_2}(150°)\,\epsilon_{\gamma_1}(90°)\times\mathrm{I}_{\gamma_2}(GATE^{90°}_{\gamma_1})$, where the quantity $\epsilon_{\gamma_1}(150°)$ is the average of the efficiencies of the rings at 146°, 149°, 156°, and 163° for the transition γ_1. Similarly, $\epsilon_{\gamma_2}(90°)$ is the average of the efficiencies of the rings at 72°, 81°, 99°, and 108° for the transition γ_2. The quantity $I_{\gamma_2}(GATE^{150°}_{\gamma_1})$ denotes the coincidence intensity of a transition γ_2, which was measured at an angle of around 150° in a spectrum gated on the transition γ_1, which in turn was detected at an angle around 90°. The quantity $I_{\gamma_2}(GATE^{90°}_{\gamma_1})$ was obtained by exchanging the angles of the gating and observed transitions. For the EUROBALL geometry and for fully aligned nuclei, a DCO ratio of 1.0 is expected if the gating and the observed transition are stretched transitions of pure and equal multipole order. $R_{DCO}=0.5$ is expected for a pure dipole transition gated on a stretched quadrupole transition. The inverse value of $R_{DCO}=2.0$ is expected for a quadrupole transition gated on a dipole transition. A value of $R_{DCO}=1.0$ or 2.0 is expected for a $\Delta I=0$ transition gated on a $\Delta I=2$ or $\Delta I=1$ transition, respectively.

The DCO ratios of most of the transitions belonging to ^{66}Ge were deduced from the DCO matrices sorted from the run with the gold-backed target. The DCO ratios of some transitions, which could not be observed or are very weakly populated, were obtained from the experiment using the self-supporting target. To deduce the DCO ratios for a number of

TABLE I. γ rays assigned to ^{66}Ge in the present experiment.

E_γ[a] (keV)	E_γ[b] (keV)	I_γ[c]	R_{DCO}[d]	Gate[e]	$\sigma\lambda$[f]	J_i^π[g]	J_f^π[h]	E_i[i] (keV)
115.4(3)		<0.1			$M1$ or $E1$	6	7^-	4204.8
125.6(2)	125.8(5)	0.7(5)			$M1$ or $E1$	12^+	11,12	7727.0
151.6(3)	151.3(6)	$0.4(^{+5}_{-1})$	0.45(20)	1074.3	$(M1)$	12^+	(11^+)	7727.0
			0.41(13)	1216.4				
173.9(2)	174.0(8)	$0.2(^{+4}_{-1})$	1.03(29)	1704.3	$M1$	8^+	8^+	5532.3
302.6(3)	302.6(6)	0.4(3)	0.90(21)	338.2	$M1$	7^-	7^-	4845.6
308.1(3)	308.0(6)	0.3(2)				9^-		5492.3
338.2(1)	338.5(3)	14.2(3)	1.02(13)	1216.4	$M1$	7^-	7^-	4543.0
			0.99(7)	521.4				
373.8(2)	374.1(4)	0.6(2)						5558.0
376.8(2)	376.6(5)	0.31(1)			$E2$	7^-	5^-	4204.8
432.5(2)	431.9(4)	1.4(2)	0.58(5)	969.8	$(M1)$	$13^{(+)}$	$12^{(+)}$	8427.2
445.4(2)	444.8(7)	0.4(3)				6		4425.4
455.0(1)	455.5(6)	4.2(2)	0.97(7)	957.7	$(M1)$	9^-	9^-	5947.3
492.2(3)	492.6(6)	2.4(2)	0.53(10)	957.7	$(M1)$	$6^{(-)}$	5^-	4320.2
506.4(2)	507.4(7)	3.6(3)	0.90(13)	521.4	$M1$	11^-	11^-	7636.7
521.4(2)	521.6(8)	85.2(8)	0.95(12)	957.7	$E2$	7^-	5^-	4204.8
			1.08(17)	1216.4				
527.1(2)	527.7(7)	0.1(5)			$(M1)$	$4^{(+)}$	3^+	3022.4
541.1(3)	541.0(5)	7.8(2)	1.07(8)	1287.5	$M1$	9^-	9^-	6033.4
548.3(2)	547.5(6)	0.6(1)	0.58(6)	969.8	$(E1)$	13^-	$12^{(+)}$	8543.0
550.8(2)	550.5(4)	0.5(1)	0.55(6)	1480.7	$E1$	7^-	6^+	4204.8
552.5(1)	552.9(4)	0.6(1)			$M1$	4^+	4^+	2725.7
583.4(3)	584.0(5)	2.3(2)	0.62(9)	1216.4	$(E1)$	$6^{(-)}$	5^+	4320.2
596.7(2)	596.2(4)[j]	0.9(1)[j]	0.62(6)	521.4	$E1$	12^+	11^-	7727.0
597.4(3)					$(E1)$	$6^{(+)}$	5^-	4425.4
603.2(2)	603.8(3)	3.1(1)	0.52(5)	1216.4	$E1$	15^-	14^+	9404.5
606.4(2)	607.1(8)	1.3(1)	0.86(17)	1216.4	$M1/E2$	11^-	11^-	7737.5
629.0(2)		<0.1					7^-	5172.0
636.8(2)	636.9(4)	1.9(1)	1.60(25)	1510.1[k]	$(M1/E2)$	$6^{(-)}$	5^-	4320.2
640.8(2)	641.4(6)	3.5(2)			$M1$	7^-	7^-	4845.6
641.2(2)	641.5(3)	3.9(4)					7^-	5184.2
661.0(2)	660.7(6)	≈ 1			$(E1)$	5^-	$4^{(+)}$	3683.4
681.2(2)	680.4(7)	≈ 1				$6^{(-)}$		4320.2
688.5(3)	689.0(7)	0.2(1)			$(M1)$	(10^-)	9^-	6635.8
688.6(3)	688.9(5)	1.2(1)	0.82(31)	956.9[k]	$(M1/E2)$	6	5^+	4425.4
688.7(2)	688.9(5)	<0.1				11^-		7636.7
695.3(3)	695.4(5)	12.6(2)	0.99(7)	956.9	$E2$	13^-	11^-	8543.0
699.9(2)	700.1(7)	0.4(2)					$10^{(+)}$	7280.8
700.2(2)	701.2(7)	3.5(2)	0.60(8)	956.9	$M1$	$13^{(+)}$	12^+	8427.2
712.3(2)	712.5(4)	1.5(1)					7^-	5558.0
714.4(2)	714.5(3)	1.7(1)	0.60(9)	1216.4[k]	$(M1)$	5^+	$4^{(+)}$	3736.8
717.7(3)	719.5(9)	0.6(1)	0.96(5)	1287.5	$M1$	11^-	11^-	7847.7
726.0(2)		<0.1			$(M1)$	9^-	(8^-)	6033.4
736.3(1)	736.3(7)	26.8(7)	0.85(12)	956.9	$M1/E2$	2^+	2^+	1693.2
742.0(2)	742.5(6)	0.8(4)	0.50(9)	956.9[k]	$M1$ or $E1$	6	5^-	4425.4
746.6(2)		<0.1					6	5172.0
758.8(2)	759.4(8)	<0.1					6	5184.2
763.1(2)	762.7(4)	1.6(2)				9^-		5947.3
786.3(3)		<0.1				6		4425.4
789.4(3)		<0.1				11^-		7737.5

TABLE I. (*Continued*).

E_γ [a] (keV)	E_γ [b] (keV)	I_γ [c]	R_{DCO} [d]	Gate [e]	$\sigma\lambda$ [f]	J_i^π [g]	J_f^π [h]	E_i [i] (keV)
802.0(1)	802.2(4)	6.0(4)	0.36(10)	956.9	$M1$	3^+	2^+	2495.4
805.5(1)	805.8(3)	3.5(3)	1.01(4)	521.4	$E2$	13^-	11^-	8543.0
805.6(2)	806.1(4)	0.7(2)			$(E1)$	5^-	$4^{(+)}$	3828.0
816.0(2)	816.8(6)	0.6(1)	0.48(10)	1224.9	$E1$	13^-	12^+	8543.0
825.8(2)	826.7(6)	1.4(1)	0.69(13)	1216.4 [k]		$13^{(+)}$	11,12	8427.2
849.1(1)	848.8(4)	3.5(2)	0.99(7)	1216.4	$(M1)$	$4^{(+)}$	4^+	3022.4
849.2(2)	849.5(6)	1.2(4)				9^-		6033.4
	(851.7(4))	< 0.1					14^+	(9653.0)
851.8(2)	852.6(6)	5.5(2)	0.88(12) [l]	969.8 [k]	$(E2)$	$13^{(+)}$	(11^+)	8427.2
852.3(5)		< 0.1				8^+		5532.3
859.6(2)	861.1(7)	4.0(2)			$E2$	7^-	5^-	4543.0
861.5(1)	861.8(4)	25.5(3)	0.92(16)	521.4 [k]	$E2$	15^-	13^-	9404.5
			1.11(16)	1287.5 [k]				
882.0(2)		< 0.1				(8^-)	6	5307.4
884.4(2)	885.6(7)	1.0(2)	0.75(17)	1074.3	$(M1)$	$15^{(+)}$	14^+	9685.7
886.5(1)	887.1(5)	9.7(2)	1.04(8)	521.4	$E2$	5^-	3^-	3683.4
906.3(1)	907.1(6)	15.4(3)	0.93(8)	956.9	$E2$	13^-	11^-	8543.0
943.2(2)		< 0.1					5^+	4680.0
949.3(2)	950.3(5)	4.5(6)	1.02(6)	338.2	$E2$	9^-	7^-	5492.3
956.9(1)	957.1(4)	140.0(3)	1.00(3)	1216.4	$E2$ [m]	2^+	0^+	956.9
957.6(2)	957.8(7)	0.3(2)					$4^{(+)}$	3980.0
957.7(2)	957.4(5)	34.9(4)	0.73(10)	1693.2	$E1$	5^-	4^+	3683.4
965.3(2)	964.9(5)	2.9(4)				11,12	(10^-)	7601.4
969.8(2)	971.4(6)	19.7(3)	0.96(3)	956.9	$E2$	10^+	8^+	6502.1
979.4(1)	981.6(4) [j]	6.4(2)					7^-	5184.2
979.0(2)		2.4(4)						6163.2
987.2(1)	987.4(3)	4.0(2)	0.89(21)	1216.4	$(E2)$	(8^-)	$6^{(-)}$	5307.4
			1.10(7)	956.9 [k]				
991.2(3)		< 0.1						6163.2
994.5(2)	995.1(5)	1.9(2)	0.58(18)	1216.4	$(M1)$	(11^+)	$10^{(+)}$	7575.4
			0.56(22)	1048.6				
1000.9(2)	1001.0(5)	0.8(6)				11^-	(10^-)	7636.7
1009.8(2)	1009.9(3)	5.5(3)	0.48(7)	521.4	$E1$	10^+	9^-	6502.1
1011.1(3)	1010.5(4)	3.2(2)			$M1$	5^+	4^+	3736.8
1015.0(2)	1015.0(5)	≈ 0.1					7^-	5558.0
1031.1(2)	1031.5(5)	2.3(2)	1.08(9)	1840.0	$E2$	5^-	3^-	3828.0
1032.4(3)	1031.8(4)	17.6(5)	1.06(5)	521.4	$E2$	4^+	2^+	2725.7
1048.6(2)	1048.5(5)	2.0(1)	0.91(12)	1216.4	$(E2)$	$10^{(+)}$	8^+	6580.9
1073.3(2)	1073.3(4)	5.9(3)			$(M1)$	(11^+)	10^+	7575.4
1074.3(1)	1074.8(4)	12.6(6)	1.01(3)	956.9	$E2$	14^+	12^+	8801.3
1102.4(2)	1102.8(6)	0.2(1)			$(M1)$	(8^-)	7^-	5307.4
1103.6(1)	1102.2(8) [j]	2.4(2) [j]	0.65(12)	1693.2	$E1$	3^-	2^+	2796.9
1132.6(3)		< 0.1					6	5558.0
1143.7(2)	1143.9(4)	16.0(3)	0.95(5)	1216.4	$E2$	10^+	8^+	6502.1
1143.8(3)		≈ 0.1					3^+	3639.2
1146.2(3)	1146.0(5)	0.2(1)				13^+		8427.2
1187.8(1)	1188.7(5)	2.1(3)	0.96(3)	1216.4	$E2$	9^-	7^-	6033.4
1216.4(1)	1217.1(6)	100(2)	1.00(3)	956.9	$E2$	4^+	2^+	2173.3
1218.3(2)	1219.2(7)	0.6(2)			$E2$	11^-	9^-	7636.7
1222.5(3)	1223.0(7)	0.2(1)				$10^{(+)}$	8^+	6580.9
1224.9(1)	1225.1(7)	20.2(7)	1.03(6)	956.9	$E2$	12^+	10^+	7727.0
	(1225.8(2))	≈ 0.1					$13^{(+)}$	(9653.0)
1241.5(2)	1241.0(4)	0.3(1)	1.32(26)	956.9 [k]	$E2$	5^+	3^+	3736.8
			2.16(25)	802.0				
1258.5(2)	1259.2(5)	3.3(2)	1.27(30)	969.8	$(E2)$	$15^{(+)}$	$13^{(+)}$	9685.7
1286.9(3)	1285.3(9)	14.0(6)	1.21(12)	338.2 [k]	$E2$	17^-	15^-	10691.4
1287.5(1)	1287.4(4)	52.6(7)	1.03(5)	956.9	$E2$	9^-	7^-	5492.3

TABLE I. (*Continued*).

E_γ [a] (keV)	E_γ [b] (keV)	I_γ [c]	R_{DCO} [d]	Gate [e]	$\sigma\lambda$ [f]	J_i^π [g]	J_f^π [h]	E_i [i] (keV)
1327.5(2)	1327.9(5)	6.2(3)	0.57(8)	969.9	$E1$	8^+	7^-	5532.3
1328.3(2)	1328.7(4)	5.3(3)	0.91(9)	987.2 [k]	$(E2)$	(10^-)	(8^-)	6635.8
1355.2(2)	1355.9(4)	5.0(3)	1.10(17)	956.9	$E2$	6^+	4^+	(4080.9)
1390.0(3)		< 0.1						6948.0
1396.7(1)	1397.1(5)		1.1(4)			$10^{(+)}$	8^+	6580.9
1404.3(1)	1403.5(7)	6.7(4)	0.92(9)	1216.4	$E2$	9^-	7^-	5947.3
1412.7(2)	1412.8(8)	5.9(3)	0.90(8)	521.4	$E2$	13^-	11^-	8543.0
1429.3(3)	1428.6(6)	2.4(2)			$E2$	11^-	9^-	7847.7
1451.4(2)	1450.7(6)	3(1)	1.10(12)	956.9	$E2$	8^+	6^+	5532.3
1451.6(2)	1450.9(5)	1(1)				(10^-)		6635.8
1473.5(3)	1475.7(8)	0.5(2)				11^-		7636.7
1480.7(1)	1482.5(8)	46.9(5)	0.97(4)	956.9	$E2$	6^+	4^+	3654.0
1484.7(2)	1485.0(6)		≈ 0.1				3^+	3980.1
1492.6(5)	1491.9(6)	4.9(8)	1.06(3)	1480.7	$(E2)$	$12^{(+)}$	10^+	7994.7
1510.1(1)	1510.8(4)	51.7(6)	0.56(2)	956.9	$E1$	5^-	4^+	3683.4
1538.4(2)	1538.6(4)	0.2(1)	0.83(7)	956.9	$M1/E2$	3^+	2^+	2495.3
1563.5(1)	1563.3(4)	1.3(1)	0.87(9)	1216.4	$M1/E2$	5^+	4^+	3736.8
1572.8(4)	1572.7(5) [j]	3.8(2)	0.91(11) [j]	956.9	$E2$	9^-	7^-	6418.4
1574.3(4)		0.8(3)				11^-		7737.5
1603.3(4)	1602.5(7)	0.7(1)			$E2$	11^-	9^-	7636.7
1620.2		< 0.1					7^-	6163.2
1638.0(2)	1638.6(4)	14.5(6)	1.04(5)	956.9	$E2$	11^-	9^-	7130.3
1654.7(2)	1655.7(8)	1.9(1)	0.54(4)	956.9	$E1$	5^-	4^+	3828.0
1672.6(1)	1672.5(4)	1.8(1)	1.16(20)	1074.3 [n]	$E2$	(16^+)	14^+	10473.9
1684.5(2)	1685.5(9)	0.3(4)				11^-		7847.7
1689.4(1)	1689.4(3)	9.1(3)	1.02(7)	1216.4	$E2$	11^-	9^-	7636.7
1693.2(1)	1694.2(9)	8.1(2)	1.05(9)	521.4	$E2$	2^+	0^+	1693.2
1704.1(2)	1704.1(3)	5.3(3)	1.03(8)	521.4	$E2$	11^-	9^-	7737.5
1704.4(2)	1704.5(4)	20.1(4)	1.01(1)	1480.7	$E2$	8^+	6^+	5358.4
1742.5(2)	1740.5(8)	0.4(2)			$E2$	9^-	7^-	5947.3
1768.8(2)	1769.1(7)	9.5(4)	1.10(4)	956.9	$E2$	4^+	2^+	2725.7
1814.3(2)	1813.5(8)	0.6(1)	1.15(32)	521.4 [j]	$E2$	11^-	9^-	7847.7
1840.0(2)	1841.9(6)	7.8(4)	0.62(11)	956.9	$E1$	3^-	2^+	2796.9
1863.4(2)	1863.9(4)	3.0(2)					$15^{(+)}$	11549.1
1878.3(2)	1880.6(8)	23.5(6)	1.02(2)	956.9	$E2$	8^+	6^+	5532.3
	1890.0(4)	1.0(5)						(13439.1)
1969.4(2)	1969.4(7)	4.0(2)	1.10(18)	1287.5 [n]	$E2$	19^-	17^-	12660.8
2245.1(2)	2244.7(3)	0.4(2)	0.95(6)	521.4	$E2$	11^-	9^-	7737.5
2355.4(3)	2357.6(9)	0.3(2)	1.02(12)	521.4	$E2$	11^-	9^-	7847.7
	2667(1)	0.2(1)	1.17(25)	1287.5 [n]	$E2$	21^-	19^-	(15328)
	2752(2)	0.2(1)	1.34(55)	1287.5 [n]	$(E2)$	(23^-)	21^-	18079

[a] γ-ray energy obtained from the experiment with the gold-backed target.

[b] γ-ray energy obtained from the experiment with the self-supporting target.

[c] Relative intensity derived from a spectrum gated on the 956.9-keV transition and normalized to intensity $I_\gamma = 100$ for the 1216.4-keV transition.

[d] DCO ratio deduced from the γ-γ matrix sorted from the backed-target experiment except for where indicated otherwise.

[e] Transition used as gate on the DCO matrix.

[f] Multipolarity compatible with the DCO ratio and the deexcitation mode.

[g] Spin and parity assignment of the initial state.

[h] Spin and parity assignment of the final state.

[i] Energy of the initial state.

[j] A combined value derived for the doublet is given.

[k] The DCO ratio was determined from the α-γ-γ matrix.

[l] May be contaminated by the intense 854-keV transition in ^{69}As, produced in one of the strongest reaction channels.

[m] Taken from Ref. [21].

[n] The DCO ratio was determined from the γ-γ matrix sorted from the self-supporting target experiment.

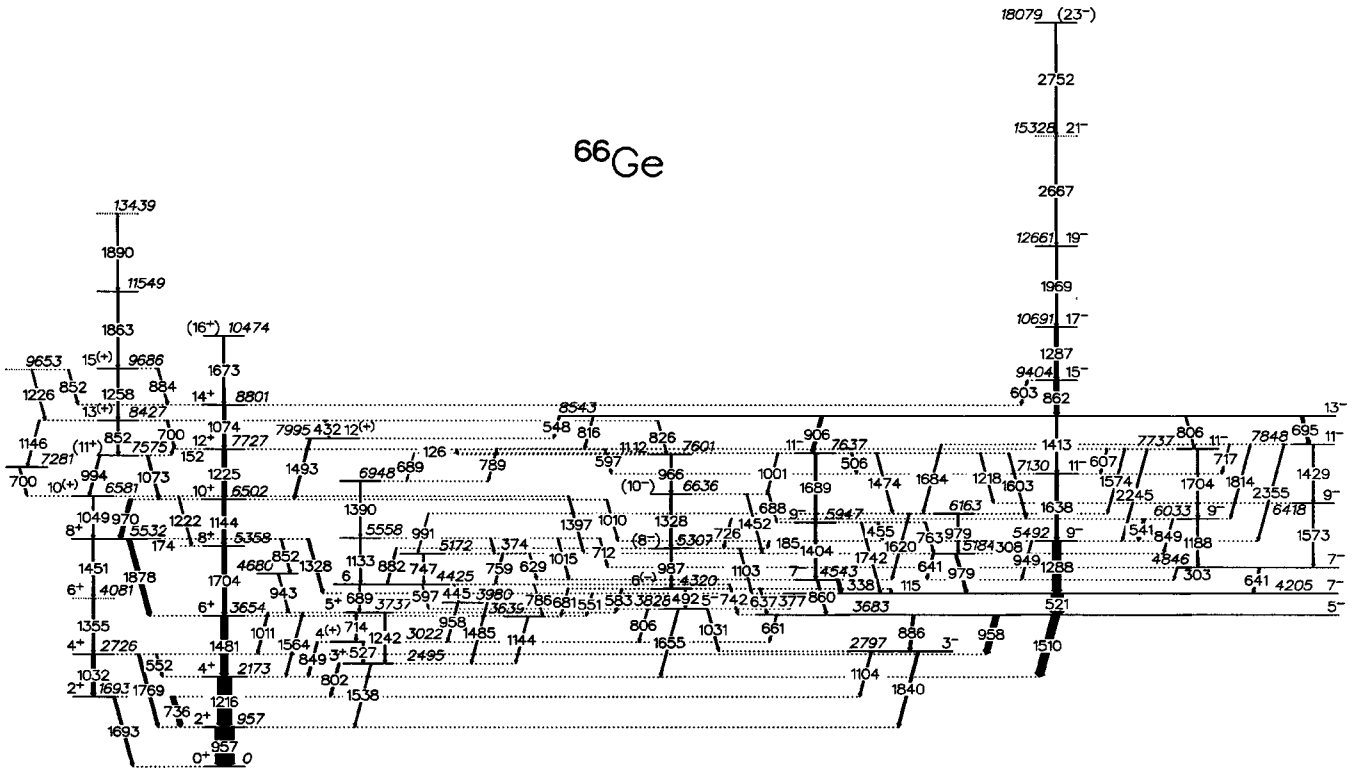

FIG. 2. Level scheme of ^{66}Ge deduced from the present experiment.

weakly populated or contaminated transitions in ^{66}Ge, different gates were used (see Table I). The corresponding coincidence spectra were extracted mainly from the γ-γ DCO matrix because of the better statistics as compared to the α-γ-γ matrix. The DCO ratios of a few contaminated transitions were derived from α-γ-γ DCO matrix. The statistics for polarization analysis was sufficient only for the strongest transitions, whose multipolarities were already known.

C. The level scheme of ^{66}Ge

The level scheme of ^{66}Ge resulting from the present experiment is shown in Fig. 2. The results of the latest in-beam study of this nucleus are presented in Ref. [13]. We extended the level scheme by two new sequences above the 6581 and 9404 keV states, respectively, and a new 1672.6-keV transition above the 8801-keV state. All states and transitions above the $I=6$ state at 4425 keV and the levels at 3639, 3980, and 4680 keV are also new.

Spin and parity of 2^+ have been assigned to the 957-keV state by Nolte *et al.* [9]. Spins and parity of $I^\pi=4^+$ and (6^+) were assigned for the 2173- and 3654-keV states, respectively, in Ref. [10] and supported in Ref. [11]. In Ref. [11], spins and parities of 2^+, 3^+, 4^+, and (5^+) were obtained for the levels at 1693, 2495, 2726, and 3737 keV, respectively. These assignments were confirmed in Ref. [13] as well as in the present work (see Table I). The DCO value obtained in the present experiment for the 849.1-keV transition points to $\Delta I=0$ character. Thus, we assigned $I=4$ to the 3022-keV state, which is in disagreement with $I^\pi=(3^-, 5^-)$ as proposed in Ref. [11]. In a two-proton transfer reaction [12], spin and parity of (4^+) were assigned to this state, in agreement with our result. The 527.1-keV transition, connecting the discussed 3022-keV state to the $I^\pi=3^+$ state at 2495 keV was found, while no branch to the $I^\pi=3^-$ state at 2797 keV was observed. Based on this, we tentatively propose positive parity for this state, although negative parity cannot be excluded. The DCO ratio of the 742.0-keV transition indicates a dipole, which results in the assignment of $I=6$ to the 4425-keV state. The DCO ratios for the 1355.2-, 1704.4-, 1451.4-, 1878.3-, 969.8-, 1143.7-, and 1224.9-keV transitions are consistent with the assignment of $I^\pi=6^+$, 8^+, 8^+, 10^+, and 12^+ to the 4081-, 5358-, 5532-, 6502-, and 7727-keV states, respectively [13]. The DCO ratios of the 1074.3- and 1492.6-keV transitions (see Table I) reveal their quadrupole nature, supporting the tentative spin and parity assignments of (12^+) and (14^+) to the 7995- and 8801-keV levels, respectively [13]. Based on the DCO ratio of the 1672.6-keV transition, we assigned $I^\pi=(16^+)$ to the 10 474-keV state. Based on the 1048.6-keV quadrupole transition, we assigned $I^\pi=10^{(+)}$ to the 6581-keV state. DCO values of 0.41(13) and 0.45(20) were obtained for the 151.6-keV transition when gating on the 1216.4- and 1074.3-keV transitions, respectively. DCO ratios of 0.56(22) and 0.58(18) were extracted for the 994.5-keV transition gating on the the 1048.6- and 1216.4-keV transitions, respectively. All these DCO ratios point to stretched $\Delta I=1$ transitions, and thus give consistent assignment of $I=11$ for the 7575-keV state. However, because of the big uncertainties, we propose the tentative $I^\pi=(11^+)$ assignment for that state. Based on the 700.2-keV dipole transition

(cf. Table I), we assigned $I^{\pi}=13^{(+)}$ to the 8427-keV state. The DCO ratio of the 851.8-keV transition may be influenced by a contamination coming from the 854-keV transition in ^{69}As, which was produced in the second strongest proton evaporation channel. The 884.4-keV transition cannot be resolved from the relatively strong 886.5-keV γ ray.

Assignments of $3^{(-)}$ and 3^{-} were made to the 2797-keV state in Refs. [11,13]. Based on the dipole character of the 1103.6- and 1840.0-keV transitions (cf. Table I) and the quadrupole character of the 886.5-keV transition depopulating the 3683-keV state with $I^{\pi}=5^{-}$ [10], we also confirm $I^{\pi}=3^{-}$ for the 2797-keV state. The DCO ratios of the 1031.1- and 1654.7-keV transitions reveal $\Delta I=2$ and $\Delta I=1$, respectively, and fix $I=5$ for the 3828-keV state. An $M2$ character of the 1031.1-keV transition and the lifetime of 0.76^{+35}_{-21} ps [21] would result in an unrealistic $B(M2)$ value of approximately 10^3 W.u. Thus, positive parity for the 3828-keV level can be ruled out, leaving $I^{\pi}=5^{-}$. Based on the DCO ratios of the 492.2-, 987.2-, and 1328.3-keV transitions, we propose spins of $I=6$, (8), and (10) for the 4320-, 5307-, and 6636-keV levels, respectively. However, assuming negative parity is rather ambiguous. Both $I=6$ states at 4425 and 4320 keV decay to the 5^{+} state at 3737 keV as well as to the 5^{-} state at 3828 keV. In addition, the 583.4-keV transition is stronger than the 688.6-keV transition. So it is not clear if the next negative-parity state above the 3828-keV level is at 4320 or 4425 keV. We propose negative parity for the 4320-keV state based on a comparison with ^{68}Ge. In addition, positive parity for the 4320-keV state would result in positive parity for the 5307-keV state. Consequently, the 5307-keV state would be the first 8^{+} state, which seems rather unlikely. On the basis of angular distribution and polarization analyses, $I^{\pi}=5^{-}$ and 7^{-} were proposed for the 3683- and 4205-keV states [10]. The $E1$ multipolarity for the 1510.1-keV transition was recently confirmed in Ref. [22]. The tentative assignment of $I^{\pi}=9^{-}$ to the 5492-keV state [10] was confirmed in Ref. [13]. The DCO ratio of the 1287.5-keV transition obtained in the present experiment (see Table I) definitely supports $I=9$ for the 5492-keV state. The negative parity of this state is strongly preferred due to its small lifetime of 2.8(3) ps [10], which excludes $M2$ character for the 1287.5-keV transition. Tentative spins and parities of (7^{-}), (9^{-}), and (11^{-}) were proposed [13] for the 4543-, 5947-, and 7637-keV sequence as well as for the 4846-, 6033-, and 7737-keV sequence. Similarly, $I^{\pi}=(11^{-})$, (11^{-}), and (13^{-}) were proposed [13] for the 7130, 7848, and 8543-keV states. As can be seen from Table I, these tentative spin assignments were confirmed by the DCO ratios extracted in the present experiment. In addition to the previous work [13], we assigned a spin of 9 to the 6418-keV state based on the DCO ratio of the 1572.8-keV transition, and we found a new 1429.3-keV transition connecting the 6418- and 7848-keV states. Due to the newly observed 859.6-keV transition, negative parity can be assigned to the 4543-keV state. In fact, the lifetime of 60(4) ps [10] would result in a $B(M2)$ value of more than 10 W.u. for the 859.6-keV transition, which we consider unlikely. Taking into account the $\Delta I=2$ cascades connecting the 7, 9, 11, and 13 levels above the 7^{-} state at 4205 keV as well as the similar decay pattern of all these states, we propose negative parity for all of them. The level at 5184 keV was assigned $I^{\pi}=(9^{-})$ in Ref. [11]. We found that the 979-keV line is an unresolved doublet and placed the second 979.0-keV transition just above the first 979.4-keV transition. No appropriate gate giving sufficient statistics to deduce the DCO ratio of one of them could be found. Thus, no spins were assigned to the 5184- and 6163-keV states. Because of the quadrupole character of the 861.5-, 1286.9-, 1969.4-, 2667-, and 2752-keV transitions, we assigned spin and parity of $I^{\pi}=15^{-}$, 17^{-}, 19^{-}, 21^{-}, and (23^{-}) to the 9404-, 10 691-, 12 661-, 15 328-, and 18 079-keV states, respectively.

Analyses of level lifetimes using the Doppler-shift attenuation method were not possible because of strong contaminations coming from the oxidized ^{40}Ca target.

III. DISCUSSION

In order to interpret the observed high-spin structure in ^{66}Ge, total Routhian surface (TRS) calculations were performed [23–25]. As there exist certain similarities to the neighboring isotope ^{68}Ge, which was studied in more detail in the past, we will discuss the relation to this nucleus as well as to its $N=Z$ neighbor ^{64}Ge. For comparison, we performed TRS calculations for ^{68}Ge as well. In order to understand the properties of the $4qp$ band in ^{66}Ge, we also refer to similar structures in near spherical and in deformed heavier nuclei ($A\approx 80$) with $N\simeq Z$.

A. Ground band, γ band and first band crossing

The lowest states in ^{66}Ge and ^{68}Ge were interpreted in Refs. [9,10,26,27] in terms of coexistent quasivibrations and quasirotations. The excited VAMPIR approach describes the positive-parity yrast states up to spin 6 in ^{68}Ge [3–5] as almost pure oblate states. This is consistent with the TRS calculations we performed for ^{68}Ge. The deepest minimum at $\hbar\omega=0$ MeV [see Fig. 3(a)] is obtained for a collective oblate shape with $\beta_2\approx 0.21$ and $\gamma\approx -51°$, and probably corresponds to the ground state. In agreement with the experiment (e.g., Refs. [13,28]), it persists up to $I\approx 6$ and $\hbar\omega=0.69$ MeV. Two prolate minima ($\beta_2\approx 0.20$ and $\gamma\approx 13°$; $\gamma\approx -15°$), separated by an energy barrier of approximately 300 keV from the deepest one, were obtained as well. Consequently, shape coexistence and γ softness have been concluded for ^{68}Ge from the TRS plot at low spin. The TR surface for ^{66}Ge gives five degenerate minima at $\hbar\omega=0$ MeV, having β_2 values in the range 0.20–0.23 and different γ values [see Fig. 3(b)], forming in this way a long valley on the TR surface. Thus, ^{66}Ge turns out to be extremely soft with respect to the triaxial deformation. In ^{66}Ge, the minimum at $\beta_2\approx 0.23$ and $\gamma\approx -54°$, persisting up to $\hbar\omega=0.79$ MeV as the deepest one, may correspond to the ground-state band. In Fig. 4, the experimental kinematic moments of inertia $J^{(1)}$ in ^{66}Ge are compared with the calculated ones. The calculated $J^{(1)}$ values for the proposed oblate ground-state band reproduce the experimental values at $\hbar\omega$

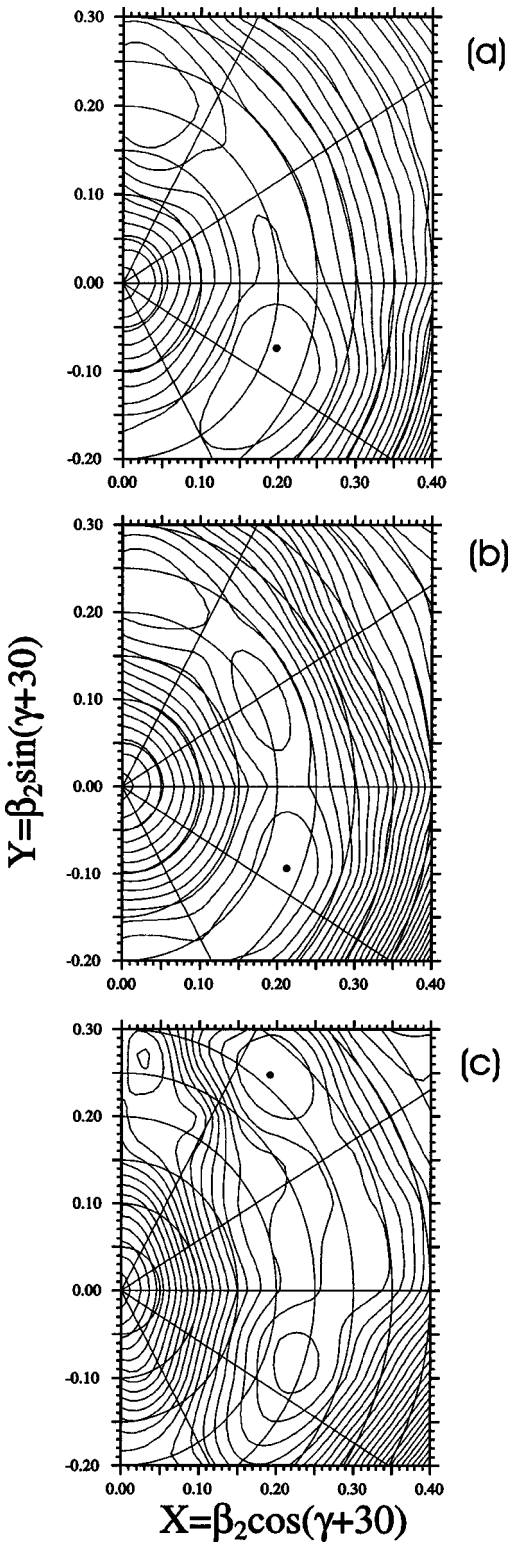

FIG. 3. Total Routhian surfaces for positive-parity states in ^{68}Ge at $\hbar\omega=0$ MeV (a), for ^{66}Ge at $\hbar\omega=0$ (b), and $\hbar\omega=0.693$ MeV (c). The energy separation between the contour lines is 200 keV.

>0.60 MeV rather well, while at lower frequencies the prolate configuration with $\beta_2\approx0.20$ and $\gamma\approx0°$ gives a slightly better agreement. The prolate minimum might correspond to the first excited band (proposed to be the favored signature

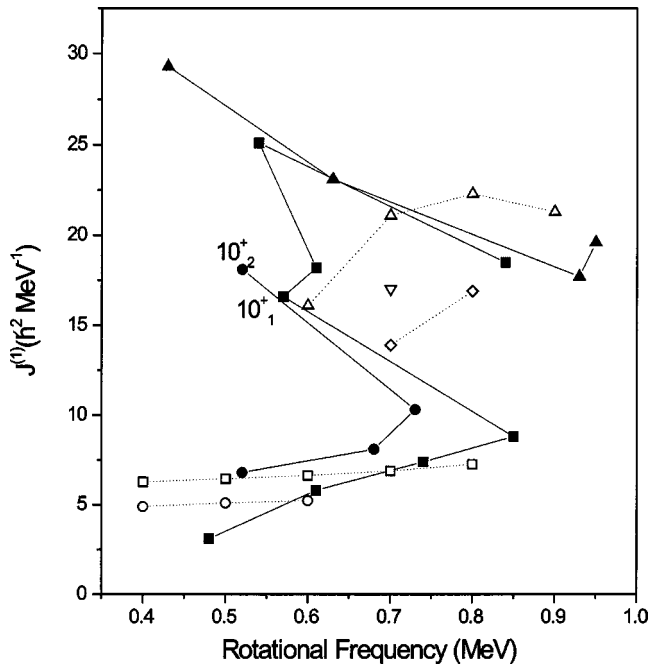

FIG. 4. Comparison of experimental (solid symbols) and theoretical (open symbols) kinematic moments of inertia for positive-parity bands in ^{66}Ge. The solid squares mark the positive-parity yrast band with even spins, the solid circles correspond to the band on top of the second 2^+ state, while the solid triangles correspond to the band on top of the $11^{(+)}$ state. The calculated moments of inertia corresponding to the oblate minimum at $\beta_2\approx0.23$, $\gamma\approx-54°$ (□), and to the prolate minimum at $\beta_2\approx0.20$, $\gamma\approx0°$ (o) are also presented. The kinematic moments of inertia of the calculated $4qp$ band with deformation parameters of $\beta_2\approx0.30$ and $\gamma\approx27°$ (△), $\beta_2\approx0.31$ and $\gamma\approx-23°$ (◇), and $\beta_2\approx0.32$ and $\gamma\approx-3.3°$ (∇) are also marked.

of the γ band) as this minimum persists to lower rotational frequency than the oblate one, which is in agreement with the experiment, where the qp alignment occurs first in this band. In Fig. 5(a), the comparison of calculated and experimental Routhians for the discussed positive-parity states shows satisfactory agreement.

We assigned the state at 3022 keV to be $4_3^{(+)}$, and the present experiment revealed very complicated connections around the 3_1^+ and 5^+ states, expected to be odd-spin members of the γ band. The insufficient experimental information hardly allows the discussion in this part of the scheme. The γ softness proposed by the calculations might be the reason for the complicated branches and connections in this region. A $(3^+, 4^+)$ and $(5^+, 6^+)$ γ-band clustering also indicates a γ-soft shape [29,30].

At $I^\pi>6^+$, the ground-state band in ^{68}Ge [13,28] forks to three 8^+ states, while only two forking branches have been observed so far in ^{66}Ge. In ^{68}Ge, almost equally strong $2qp$ contributions from aligned $g_{9/2}$ neutrons and protons to the 8_1^+ state and a $\nu(g_{9/2}^2)$ configuration to the 8_2^+ state were proposed [5,13,31], while the 8_3^+ state was interpreted as the continuation of the oblate ground band [5,13,27]. In contrast to ^{68}Ge, where the yrast sequence exhibits irregular energy

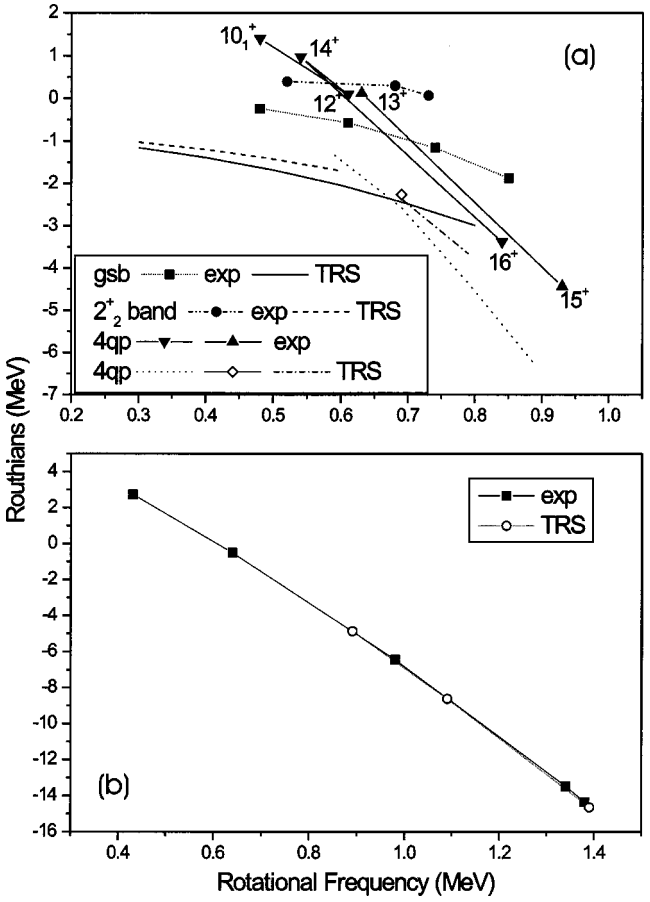

FIG. 5. Comparison of the experimental and calculated Routhians for the positive-parity states (a), and for the negative-parity states above the 13^- state (b), in ^{66}Ge.

spacings just above the 6^+ state, the yrast band in ^{66}Ge shows an irregularity above the 8^+ state. Calculations exploiting IBM with an unpaired fermion pair [32] predict two aligned $g_{9/2}^2$ nucleons for the 8_1^+ and 10_1^+ states in ^{66}Ge. On the other hand, IBM and $2qp$-plus-rotor model calculations [11] describe the 8_1^+ state as the continuation of the ground band, while in the 8_2^+ and 10_1^+ states the aligned $\pi(g_{9/2}^2)$ configuration should dominate. In two-proton transfer reactions [12], a $\nu(g_{9/2}^2)$ configuration was assigned to the 8_2^+ state at 5.50 MeV in ^{66}Ge. The $J^{(1)}(\omega)$ plot shown in Fig. 4 suggests the 8_1^+ state to belong to the ground-state band. This is supported by the observation of the 8^+ member of the ground-state band in ^{68}Ge [5,13] at almost the same energy (5367 keV). This argument can be used, since the energies of the ground-state band members in ^{66}Ge and ^{68}Ge are very similar with a maximum difference of only 100 keV. The TRS calculations also predict the ground-state band in ^{66}Ge to be yrast up to a higher rotational frequency than in ^{68}Ge. The first band crossing cannot be followed in the present TRS calculations for ^{66}Ge, because the second alignment occurs immediately after the first one. In fact, the TRS calculations performed for several nuclei near the $N=Z$ line, e.g., in ^{70}Se [33], ^{72}Kr [34], ^{76}Kr [35], and now in ^{68}Ge, predict simultaneous alignment of protons and neutrons at the first band crossing. This is due to the fact that neutrons and protons occupy the same orbitals and strongly mix.

B. Four-quasiparticle positive-parity regime

1. Structures with staggered M1 transitions in A≈80 nuclei

Above spin 10, the newly observed positive-parity yrast sequence in ^{66}Ge differs from that in ^{68}Ge [13,28] as well as from that in the heavier Ge isotopes, where rotationally aligned $\Delta I=2$ bands develop. Instead, a cascade of $\Delta I=1$ $M1$ transitions connecting two $\Delta I=2$ sequences was observed. Their energy staggering does not give any indication of a strongly coupled band. Actually, this structure is very similar to the level structures above the 12_1^+ states in the $N=46$ isotones ^{84}Sr [36], ^{86}Zr [36–38], ^{88}Mo [36], and partially in ^{90}Ru [39]. Lifetime measurements revealed that the observed $M1$ staggering in the $4qp$ structures in these latter nuclei is due to the sequence of transitions with moderate $B(M1)$ strength around 0.1 W.u. and rather strong transitions with $B(M1)>0.5$ W.u. The lower sequences in these nuclei point to nearly spherical shapes [2,36,38–42], but $2qp$ $g_{9/2}^2$ alignment forces them to more deformed shapes, e.g., Ref. [2], while the subsequent $4qp$ $\pi(g_{9/2}^2)\nu(g_{9/2}^2)$ aligned configuration was proposed to drive the nuclei again to less deformed, even near-spherical shapes [36,38,39,43]. The recoupling of spins in such a spherical $\pi(g_{9/2}^2)\nu(g_{9/2}^2)$ high-j configuration is proposed to explain [36,38,39,43] the observed $M1$ energy and strength staggering. The $N=44$ isotones ^{86}Mo [40,44] and ^{84}Zr [45] reveal deformed ground-state bands. However, similar to the discussed $N=46$ isotones, a level sequence interpreted as being due to a strong influence of the shell model $\pi(g_{9/2}^2)\nu(g_{9/2}^2)$ configuration [44] was observed on top of the 14_2^+ state in ^{86}Mo. A part of similar level sequence above the 14_2^+ state was observed as well in ^{84}Zr [45]. Consequently, in the $4qp$ region, the deformed $N=44$ nuclei ^{86}Mo and ^{84}Zr closely resemble the near-spherical at low spin $N=46$ isotones ^{84}Sr, ^{86}Zr, ^{88}Mo, and ^{90}Ru. On the other hand, $4qp$ rotational aligned $\Delta I=2$ bands develop, for example, in the $N=44$ and $N=46$ nuclei ^{80}Kr [46] and ^{82}Kr [47]. The TRS calculations for ^{80}Kr [48] predict that $4qp$ alignment drives the nucleus to a smaller deformation, but not to sphericity. The reason causing the different $4qp$ characteristics in the discussed nuclei does not appear to be fully understood yet.

Experimental $B(E2)$ values reveal considerable deformation in structures with staggered $M1$ transitions involved and based on the $\pi g_{9/2}\nu g_{9/2}$ configuration in a number of odd-odd nuclei with $A\approx 70$–80. Based on two-noninteracting-quasiparticle plus rotor calculations, these bands were interpreted as Coriolis distorted [49]. They were described to emerge [49,50] from the strong Coriolis mixing acting on the high-j band configurations. The fact that rotational aligned $\Delta I=2$ bands (instead of Coriolis distorted) based on the same configuration were observed, on the other hand, in neighboring nuclei was explained with the different positions of the neutron and proton Fermi levels [49]. Two-quasiparticle plus triaxial rotor calculations describe the strong $M1$ transitions as being due to a change of the cou-

pling between the quasiparticles and the core, while the weaker are only due to changes in the core rotational states, and the calculated wave functions reveal strong K mixing [51–53]. In Ref. [54], the possibility of describing the enhancement of the $M1$ strength with cranking approximations is presented. The signature dependence of the $\Delta I=1$ transitions is discussed in Refs. [54,55]. In addition to the staggered $M1$ transitions, the so called signature inversion was observed in most (probably even in all) bands in odd-odd nuclei. A list of different explanations of this phenomenon can be found in Refs. [53,56,57]. Although a big amount of experimental results is consistently reproduced by the model calculations, no definite conclusion was drawn about the deformation and the positions of proton and neutron Fermi levels, at which so called Coriolis-distorted structures may emerge in $A\approx 80$ nuclei. Also, different reasons may explain the signature inversion in different structures depending on the deformation and Fermi positions.

2. Deformed 4qp structure in ^{66}Ge

A level sequence with energetically staggered $M1$ transitions was found in ^{66}Ge in a spin region where the $4qp$ regime is expected. Its similarity with the $4qp$ structures in the $N=44$ and $N=46$ Sr, Mo, Zr, and Ru isotones discussed before suggests a noticeable decrease of deformation. However, at $I\approx 9-10$, e.g., immediately after the first band crossing in ^{66}Ge, two minima very close in energy at $\hbar\omega=0.59$ MeV ($\beta_2\approx 0.30$, $\gamma\approx 27°$) and $\hbar\omega=0.69$ MeV ($\beta_2\approx 0.31$ and $\gamma\approx -23°$), result in the TRS calculations [see Fig. 3(c)] corresponding to $4qp$ configurations with different degrees of aligned protons and neutrons. Thus, the TRS calculations predict that the $4qp$ $\pi(g_{9/2}^2)\nu(g_{9/2}^2)$ alignments drive the nucleus to considerable triaxial deformation. We determined experimental $B(M1)/B(E2)$ ratios for the newly observed level sequence with energy staggered $M1$ transitions in ^{66}Ge directly from the energies of the $M1$ and $E2$ transitions and the branching ratios λ, neglecting possible $E2/M1$ mixing ratios δ, which appear to be rather small in this kind of bands. In Fig. 6, these ratios for ^{66}Ge are compared with the ones determined from lifetime measurements in ^{86}Zr [38] and ^{72}As [58]. The $B(M1)/B(E2)$ ratios for ^{66}Ge are similar to those in the deformed ^{72}As [58,59], and are a factor of 4 lower than those in the near-spherical ^{86}Zr [36,38]. From that, a rather strong deformation can be concluded for the $4qp$ region in ^{66}Ge as well, which is consistent with the TRS predictions. To our knowledge, this is the first observation of staggered $M1$ transitions within a deformed $4qp$ $\pi(g_{9/2}^2)\nu(g_{9/2}^2)$ structure. It should be noticed that there is some difference between this structure and the deformed bands in odd-odd nuclei (see preceding section), which show a relatively regular increase of the energies of the $E2$ transitions in both sequences interpreted as signature partners. However, the even spin sequence in ^{66}Ge above 10_1^+ state reveals rather irregular level spacings, suggesting possible band crossings. The same can be seen in Fig. 5, where the experimental Routhians show nonstable band configuration for this sequence up to the 14^+ state.

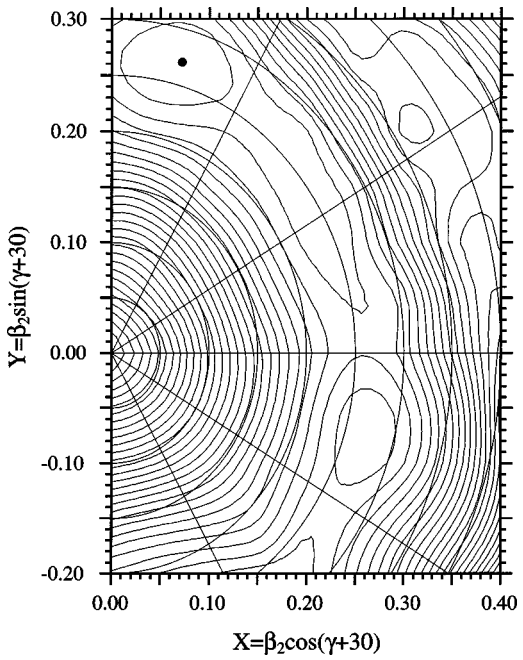

FIG. 6. Total Routhian surface of negative-parity states in ^{66}Ge at $\hbar\omega\approx 0$ MeV. The energy distance between the contour lines is 200 keV.

The TRS calculations describe the staggered $M1$ structure in ^{66}Ge as due to triaxial softness in the $g_{9/2}$ proton-neutron $4qp$ regime. The configuration, corresponding to the first minimum (see the beginning of this section) is mainly due to not fully aligned neutrons at $\hbar\omega=0.59$ MeV, while another one is due to almost equally partially aligned protons and neutrons, and is energetically slightly favored around spin 10. The TRS calculations for ^{66}Ge predict a complicated picture of competing $4qp$ configurations for $I^\pi>10^+$ whose γ changes along the discussed structure from negative to positive values. For example, at $\hbar\omega=0.69$ MeV, a third minimum appears at $\beta_2\approx 0.32$ and $\gamma\approx -3°$. It exists only at that frequency and corresponds to $I\approx 11-12$. Then, the configuration corresponding to the minimum at negative γ values is favored up to its crossing at spin around 14 by the configuration corresponding to the minimum at $\gamma\approx 27°$ which dominates in the positive-parity yrast structure up to its termination at spin of approximately 23–24. The change of the alignment of the quasiparticles along the band structure may produce states with j and j-1. From the combination of the latter with the high-j nature of the quasiparticles, strong $M1$ transitions may occur. It should be mentioned that in agreement with the experiment, the TRS calculations predict a rather different structure for the $4qp$ regime in ^{64}Ge and ^{68}Ge, where a rather well-deformed triaxial minimum at $\gamma\approx 30°$ and two minima at $\gamma\approx 0°$, 60° are obtained, respectively. The calculated kinematic moments of inertia $J^{(1)}$ for these configurations in ^{66}Ge are shown in Fig. 4. At lower spin they underestimate the experimental $J^{(1)}$ values, while at higher spin the predicted stabilization of one of the configurations is in good agreement with the experiment. It can be seen from Fig. 4 that to reproduce the trend of the experimental $J^{(1)}$ with these configurations, complicated crossings

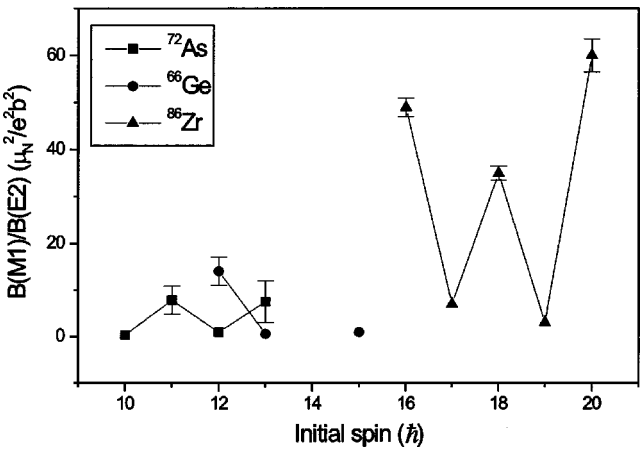

FIG. 7. Comparison of the experimental $B(M1)/B(E2)$ ratios within the discussed $M1$ staggered sequence in ^{66}Ge (dots) with those in ^{72}As [58] (squares) and ^{86}Zr (triangles) [38]. The $B(M1)/B(E2)$ ratios in ^{66}Ge are obtained assuming $E2/M1$ mixing ratios $\delta=0$ for the $\Delta I = 1$ transitions.

and probably mixing between them may occur. A comparison between calculated and experimental Routhians [see Fig. 5(a)] again points to crossings between $\pi(g_{9/2}^2)\nu(g_{9/2}^2)$ configurations with different alignments corresponding to different minima.

C. Negative-parity bands

The 3^- state at 2797-keV fits into the systematics of octupole vibrations in the Ge isotopes [10,60,61]. Based on $2qp$ plus rotor calculations [11], the 5^- state at 3683 keV in ^{66}Ge was interpreted as a partially aligned $\pi(g_{9/2},p_{3/2})$ state, while for the first 7^- state and for the band on top of it, a more completely aligned $\pi(g_{9/2},f_{5/2})$ configuration was predicted. These calculations put a second less aligned proton band, built on top of a 7^- state as well as an aligned two-quasineutron band at almost the same energies [11], and finally a proton or a proton-neutron $2qp$ configuration for the second experimental negative-parity band in this spin-energy region.

As in the case of positive parity, the TRS calculations predict five minima near $\hbar\omega=0$ MeV (cf. Fig. 7). The deepest one at $\beta_2\approx0.27$ and $\gamma\approx45°$ is predicted at a spin of approximately 3, in agreement with the experiment. A sixth minimum, separated from the others by an energy barrier of about 2 MeV refers to the superdeformed shape of $\beta_2\approx0.42$ and $\gamma\approx-2.5°$. Note that a superdeformed band was observed in ^{68}Ge [28]. Aligned pair of quasineutrons is predicted for the first 7^-, 9^-, and 11^- band, in disagreement with the quasiparticle plus rotor model calculations [11] (see above), where a $2qp$ aligned proton configuration was proposed for the energetically most favored negative-parity band. In agreement with our calculations, neutron character was assigned to the first 7^- state in a two-proton transfer experiment [12]. The proposed [12] proton character for the second 7^- state is again consistent with our calculations. However, the neutron alignment wins in others calculated bands and most of the bandhead configurations are mainly differently aligned $(p_{3/2}f_{5/2};g_{9/2})^2$ quasineutrons. To describe the experimental states with the present calculations, complicated crossings along the observed bands with differently aligned bands should be assumed. Considering the predicted shape parameters for the different band configurations, this points to a strong competition between collective and noncollective configurations with different deformations. In addition to the predicted crossings, the complicated experimentally observed $\Delta I=0$ $M1$ and $\Delta I=2$ $E2$ linking transitions between the different bands reveal a strong band mixing. Taking into account the variety of shapes and collective and noncollective degrees of freedom predicted by the TRS calculations for the spin region between 3^- and 13^- states, shape mixing is very likely. A deformation $\beta_2\approx0.28$–0.30 and $\gamma=60°$ is predicted by the present calculations for the newly observed band on top of the 13^- state. Above $I^\pi=15^-$, it is nicely reproduced [see Fig. 5(b)] by the aligned $\nu(g_{9/2}^2)\pi(p_{3/2}f_{5/2};g_{9/2})^2$ configuration. The minimum persists up to angular momentum $28\hbar$, while the $\nu(g_{9/2}^2)\pi(p_{3/2}f_{5/2};g_{9/2})^2$ band terminates at spin around $20\hbar$–$21\hbar$, in agreement with the experiment, revealing a possible crossing above the 21^- state. Cranked Nilsson-Strutinski model calculations [28], performed for the very similar band on top of the 13^- state in ^{68}Ge [28], predict that it terminates at 23^- having $\epsilon_2\approx0.24$ and $\gamma=60°$ with a $\nu(g_{9/2})^2(f_{5/2},p_{3/2})^6\pi(g_{9/2})^1(f_{5/2},p_{3/2})^3$ configuration. Both calculations predict almost the same deformations and configurations for the bands on top of the 13^- states in ^{66}Ge and ^{68}Ge.

IV. SUMMARY

The $N=Z+2$ nucleus ^{66}Ge was populated via the reaction ^{40}Ca(^{32}S,$\alpha2p$) at beam energies of 105 and 95 MeV. The EUROBALL array, combined with the 4π charged-particle array EUCLIDES and the neutron wall was used. The level scheme of ^{66}Ge was extended up to $E\approx18$ MeV. On the basis of DCO analyses, spin assignments to most of the new levels were possible, and a number of previous assignments could be confirmed or rejected. Based on the many parallel decays, tentative assignments of the parities of the observed states were made.

To interpret their structures, total Routhian surface calculations were performed. They describe ^{66}Ge at low spin as a γ-soft nucleus with a moderate deformation of $\beta_2\approx0.23$. Above angular momentum 10 we found a positive-parity level sequence, which resembles a band with two signature partners, connected by energetically staggered $\Delta I=1$ $M1$ transitions. In contrast to the $N=44,46$ isotones ^{84}Zr, ^{86}Mo, ^{84}Sr, ^{86}Zr, ^{88}Mo, and ^{90}Ru [36,37,39,40,44,45], where very similar structures were interpreted as being due to a strong influence of the spherical $\pi(g_{9/2}^2)\nu(g_{9/2}^2)$ configuration, the TRS calculations for ^{66}Ge predict a competition and probably mixing between the same $4qp$ band configurations with different alignments and considerable triaxiality, changing in this way the γ deformation along the structure. The predicted strong deformation is supported by the estimated $B(M1)/B(E2)$ values. Then, the staggered $M1$ transitions

may occur between states with a strong contribution of aligned high-j quasiparticles having angular momenta j and $j-1$. To our knowledge, this is the first observation of a strongly deformed $4qp$ structure with staggered $M1$ transitions. Lifetime measurements could test the suggested strong deformation.

A number of $(p_{1/2}p_{3/2}f_{5/2},g_{9/2})^2$ configurations (mainly quasineutrons) with different alignments and deformation parameters were calculated in the spin region between 3^- and 13^-. They again reveal a strong competition between collective and noncollective degrees of freedom, different shapes, as well as a possible mixing between them. An aligned $\nu(g_{9/2}^2)\pi(p_{3/2}f_{5/2},g_{9/2})^2$ configuration with $\beta_2\approx 0.29$ and $\gamma = 60°$ was calculated for the newly observed band on top of the 15^- state. The TRS calculations also predict a negative-parity superdeformed band in ^{66}Ge, similar to the one observed in ^{68}Ge [28], but not in ^{66}Ge yet.

ACKNOWLEDGMENTS

This work was supported by BMBF 06 GÖ 951 and TMR/LSF Contract No. HPRI-CT-1999-00078. The authors are indebted to the crew of the VIVITRON accelerator and the EUROBALL facility at IReS for their dedicated efforts and cooperation.

[1] R. Bengtsson, P. Möller, J.R. Nix, and J. Zhang, Phys. Scr. **29**, 402 (1984).
[2] W. Nazarewicz, J. Dudek, R. Bengtsson, T. Bengtsson, and I. Ragnarsson, Nucl. Phys. **A435**, 397 (1985).
[3] A. Petrovici, K.W. Schmid, F. Grümer, and A. Faessler, Nucl. Phys. **A504**, 277 (1989).
[4] A. Petrovici, K.W. Schmid, F. Grümer, and A. Faessler, Nucl. Phys. **A517**, 108 (1990).
[5] L. Chaturvedi, X. Zhao, A.V. Ramayya, J.H. Hamilton, J. Kormicki, S. Zhu, C. Girit, H. Xie, W.-B. Gao, Y.-R. Jiang, A. Petrovici, K.W. Schmid, A. Faessler, N.R. Johnson, C. Baktash, I.Y. Lee, F.K. McGowan, M.L. Halbert, M.A. Riley, J.H. McNeill, M.O. Kortelahti, J.D. Cole, R.B. Piercey, and H.Q. Jin, Phys. Rev. C **43**, 2541 (1991).
[6] J.P. Elliott, J.A. Evans, V.S. Lac, and G.L. Long, Nucl. Phys. **A609**, 1 (1996).
[7] P.J. Ennis, C.J. Lister, W. Gelletly, H.G. Price, B.J. Varley, P.A. Butler, T. Hoare, S. Cwiok, and W. Nazarewicz, Nucl. Phys. **A535**, 392 (1991).
[8] M. Yamagami, K. Matsuyanagi, and M. Matsuo, Nucl. Phys. **A693**, 579 (2001).
[9] E. Nolte, Y. Shida, W. Kutschera, R. Prestele, and H. Morinaga, Z. Phys. **268**, 267 (1974).
[10] L. Cleemann, J. Eberth, W. Neumann, W. Wiehl, and V. Zobel, Nucl. Phys. **A334**, 157 (1980).
[11] R. Soundranayagam, R.B. Piercey, A.V. Ramayya, J.H. Hamilton, A.Y. Ahmed, H. Yamada, C.F. Maguire, G.L. Bomar, R.L. Robinson, and H.J. Kim, Phys. Rev. C **25**, 1575 (1982).
[12] A. Boucenna, L. Kraus, I. Linck, and Tsan Ung Chan, Phys. Rev. C **42**, 1297 (1990).
[13] U. Hermkens, F. Becker, J. Eberth, S. Freund, T. Mylaeus, S. Skoda, W. Teichert, and A.v.d. Werth, Z. Phys. A **343**, 371 (1992).
[14] J. Simpson, Z. Phys. A **358**, 139 (1997).
[15] A. Gadea, E. Farnea, G. de Angelis, R. Isocrate, A. Buscemi, P. Pavan, A. Algora, N. Marginean, T. Martinez, D.R. Napoli, M. De Poli, P. Spolaore, D. Bazzacco, F. Brandolini, S.M. Lenzi, S. Lundardi, R. Menegazzo, C. Rossi Alvarez, P.G. Bizzeti, A.M. Bizzeti-Sona, and EUROBALL IV Collaboration, LNL Annual Report No. 151, 1999, INFN(REP) 160/00.
[16] Ö. Skeppstedt, H.A. Roth, L. Lindstrom, R. Wadsworth, I. Hibbert, N. Kelsall, D. Jenkins, H. Grawe, M. Gorska, M. Moszynski, Z. Sujkowski, D. Wolski, M. Kapusta, M. Hellstrom, S. Kalogeropoulos, D. Oner, A. Johnson, J. Cederkäll, W. Klamra, J. Nyberg, M. Weiszflog, J. Kay, R. Griffiths, J. Garces Narro, C. Pearson, and J. Eberth, Nucl. Instrum. Methods Phys. Res. A **421**, 531 (1999).
[17] D.C. Radford, Nucl. Instrum. Methods Phys. Res. A **361**, 297 (1995).
[18] R.M. Steffen and K. Alder, in *The Electromagnetic Interaction in Nuclear Spectroscopy*, edited by W.D. Hamilton (North-Holland, Amsterdam, 1975), p. 505.
[19] K.S. Krane, R.M. Steffen, and R.M. Wheeler, Nucl. Data Tables **11**, 351 (1973).
[20] A. Krämer-Flecken, T. Morek, R.M. Lieder, W. Gast, G. Hebbinghaus, H.M. Jäger, and W. Urban, Nucl. Instrum. Methods Phys. Res. A **275**, 333 (1989).
[21] M.R. Bhat, Nucl. Data Sheets **83**, 789 (1998).
[22] E. Farnea, G. de Angelis, A. Gadea, P.G. Bizzeti, A. Dewald, J. Eberth, A. Algora, M. Axiotis, D. Bazzacco, A.M. Bizzeti-Sona, F. Brandolini, G. Colo, W. Gelletly, M.A. Kaci, N. Kintz, T. Klug, Th. Kröll, S.M. Lenzi, S. Lunardi, N. Marginean, T. Martinez, R. Menegazzo, D.R. Napoli, J. Nyberg, P. Pavan, Zs. Podolyák, C.M. Petrache, B. Quintana, B. Rubio, P. Spolaore, Th. Steinhardt, J.L. Tain, O. Thelen, C.A. Ur, R. Venturelli, and M. Weiszflog, Phys. Lett. B **551**, 56 (2003).
[23] W. Satula, R. Wyss, and P. Magierski, Nucl. Phys. **A578**, 45 (1994).
[24] W. Satula and R. Wyss, Phys. Rev. C **50**, 2888 (1994).
[25] W. Satula and R. Wyss, Phys. Scr. **T56**, 159 (1995).
[26] R.C. Pardo, C.N. Davids, M.J. Murphy, E.B. Norman, and L.A. Parks, Phys. Rev. C **15**, 1811 (1977).
[27] A.P. de Lima, A.V. Ramayya, J.H. Hamilton, B. Van Nooijen, R.M. Ronningen, H. Kawakami, R.B. Piercey, E. de Lima, R.L. Robinson, H.J. Kim, L.K. Peker, F.A. Rickey, R. Popli, A.J. Caffrey, and J.C. Wells, Phys. Rev. C **23**, 213 (1981).
[28] D. Ward, C.E. Svensson, I. Ragnarsson, C. Baktash, M.A. Bentley, J.A. Cameron, M.P. Carpenter, R.M. Clark, M. Cromaz, M.A. Deleplanque, M. Devlin, R.M. Diamond, P. Fallon, S. Flibotte, A. Galindo-Uribarri, D.S. Haslip, R.V.F. Janssens, T. Lampman, G.J. Lane, I.Y. Lee, F. Lerma, A.O. Macchiavelli, S.D. Paul, D. Radford, D. Rudolph, D.G. Sarantites, B. Schaly, D. Seweryniak, F.S. Stephens, O. Thelen, K. Vetter, J.C. Wad-

dington, J.N. Wilson, and C.-H. Yu, Phys. Rev. C **63**, 014301 (2001).
[29] L. Wilets and M. Jean, Phys. Rev. **102**, 788 (1956).
[30] N. Yoshikawa, Y. Shida, O. Hashimoto, M. Sakai, and T. Numao, Nucl. Phys. **A327**, 477 (1979).
[31] M.E. Barclay, J. Phys. G **12**, L295 (1986).
[32] S.T. Hsieh, H.C. Chiang, and Der-San Chuu, Phys. Rev. C **46**, 195 (1992).
[33] T. Mylaeus, J. Busch, J. Eberth, M. Liebchen, R. Sefzig, S. Skoda, W. Teichert, M. Wiosna, P. von Brentano, K. Schiffer, K.O. Zell, A.V. Ramayya, K.H. Maier, H. Grawe, A. Kluge, and W. Nazarewicz, J. Phys. G **15**, L135 (1989).
[34] G. de Angelis, C. Fahlander, A. Gadea, E. Farnea, W. Gelletly, A. Aprahamian, D. Bazzacco, F. Becker, P.G. Bizzeti, A. Bizzeti-Sona, F. Brandolini, D. de Acuna, M. De Poli, J. Eberth, D. Foltescu, S.M. Lenzi, S. Lunardi, T. Martinez, D.R. Napoli, P. Pavan, C.M. Petrache, C. Rossi Alvarez, D. Rudolph, B. Rubio, W. Satula, S. Skoda, P. Spolaore, H.G. Thomas, C.A. Ur, and R. Wyss, Phys. Lett. B **415**, 217 (1997).
[35] C.J. Gross, J. Heese, K.P. Lieb, S. Ulbig, W. Nazarewicz, C.J. Lister, B.J. Varley, J. Billowes, A.A. Chishti, J.H. McNeill, and W. Gelletly, Nucl. Phys. **A501**, 367 (1989).
[36] C.J. Lister, P. Chowdhury, and D. Vretenar, Nucl. Phys. **A557**, 361 (1993).
[37] J. Döring, Y.A. Akovali, C. Baktash, F.E. Durham, C.J. Gross, P.F. Hua, G.D. Johns, M. Korolija, D.R. LaFosse, I.Y. Lee, A.O. Macchiavelli, W. Rathbun, D.G. Sarantites, D.W. Stracener, G.Z. Solomon, S.L. Tabor, A. Vander Molen, A.V. Afanasjev, and I. Ragnarsson, Phys. Rev. C **61**, 034310 (2000).
[38] P. Chowdhury, C.J. Lister, D. Vretenar, Ch. Winter, V.P. Janzen, H.R. Andrews, D.J. Blumenthal, B. Crowell, T. Drake, P.J. Ennis, A. Galindo-Uribarri, D. Horn, J.K. Johansson, A. Omar, S. Pilotte, D. Prevost, D. Radford, J.C. Waddington, and D. Ward, Phys. Rev. Lett. **67**, 2950 (1991).
[39] J. Heese, H. Grawe, K.H. Maier, R. Schubart, F. Cristancho, C.J. Gross, A. Jungclaus, K.P. Lieb, D. Rudolph, J. Eberth, and S. Skoda, Phys. Rev. C **49**, 1896 (1994).
[40] C.J. Gross, W. Gelletly, M.A. Bentley, H.G. Price, J. Simpson, K.P. Lieb, D. Rudolph, J.L. Durell, B.J. Varley, and S. Rastikerdar, Phys. Rev. C **44**, R2253 (1991).
[41] A.W. Mountford, T. Vass, G. Kumbartzki, L.A. Bernstein, N. Benczer-Koller, R. Tanczyn, C.J. Lister, P. Chowdhury, and S.J. Freeman, Phys. Rev. C **51**, 513 (1995).
[42] R.A. Kaye, J.B. Adams, A. Hale, C. Smith, G.Z. Solomon, S.L. Tabor, G. Garcia-Bermudez, M.A. Cardona, A. Filevich, and L. Szybisz, Phys. Rev. C **57**, 2189 (1998).
[43] E. Galindo, A. Jungclaus, and K.P. Lieb, Eur. Phys. J. A **9**, 439 (2000).
[44] D. Rudolph, C.J. Gross, Y.A. Akovali, C. Baktash, J. Doring, F.E. Durham, P.-F. Hua, G.D. Johns, M. Korolija, D.R. LaFosse, I.Y. Lee, A.O. Macchiavelli, W. Rathbun, D.G. Sarantites, D.W. Stracener, S.L. Tabor, A.V. Afanasjev, and I. Ragnarsson, Phys. Rev. C **54**, 117 (1996).
[45] H.-Q. Jin, C. Baktash, M.J. Brinkman, C.J. Gross, D.G. Sarantites, I.Y. Lee, B. Cederwall, F. Cristancho, J. Doring, F.E. Durham, P.-F. Hua, G.D. Johns, M. Korolija, D.R. LaFosse, E. Landulfo, A.O. Macchiavelli, W. Rathbun, J.X. Saladin, D.W. Stracener, S.L. Tabor, and T.R. Werner, Phys. Rev. Lett. **75**, 1471 (1995).
[46] J. Döring, V.A. Wood, J.W. Holcomb, G.D. Johns, T.D. Johnson, M.A. Riley, G.N. Sylvan, P.C. Womble, and S.L. Tabor, Phys. Rev. C **52**, 76 (1995).
[47] P. Kemnitz, P. Ojeda, J. Döring, L. Funke, L.K. Kostov, H. Rotter, E. Will, and G. Winter, Nucl. Phys. **A425**, 493 (1984).
[48] G. Mukherjee, H.C. Jain, R. Palit, P.K. Joshi, S.D. Paul, and S. Nagraj, Phys. Rev. C **64**, 034316 (2001).
[49] A.J. Kreiner and M.A.J. Mariscotti, Phys. Rev. Lett. **43**, 1150 (1979).
[50] E. Nolte and P. Vogt, Z. Phys. A **275**, 33 (1975).
[51] S. Chattopadhyay, H.C. Jain, S.D. Paul, J.A. Sheikh, and M.L. Jhingan, Phys. Rev. C **49**, 116 (1994).
[52] P.C. Womble, J. Döring, T. Glasmacher, J.W. Holcomb, G.D. Johns, T.D. Johnson, T.J. Petters, M.A. Riley, V.A. Wood, S.L. Tabor, and P. Semmes, Phys. Rev. C **47**, 2546 (1993).
[53] J. Döring, D. Ulrich, G.D. Johns, M.A. Riley, and S.L. Tabor, Phys. Rev. C **59**, 71 (1999).
[54] F. Dönau, Nucl. Phys. **A471**, 469 (1987).
[55] G.B. Hagemann and I. Hamamoto, Phys. Rev. C **40**, 2862 (1989).
[56] R. Zheng, S. Zhu, N. Cheng, and J. Wen, Phys. Rev. C **64**, 014313 (2001).
[57] B. Cederwall, F. Liden, A. Johnson, L. Hildingsson, R. Wyss, B. Fant, S. Juutinen, P. Ahonen, S. Mitarai, J. Mukai, J. Nyberg, I. Ragnarsson, and P.B. Semmes, Nucl. Phys. **A542**, 454 (1992).
[58] J. Döring, S.L. Tabor, J.W. Holcomb, T.D. Johnson, M.A. Riley, and P.C. Womble, Phys. Rev. C **49**, 2419 (1994).
[59] D. Sohler, Zs. Podolyák, Zs. Dombrádi, J. Gulyás, A. Algora, S. Brant, V. Krstić, and V. Paar, Phys. Rev. C **59**, 1328 (1999).
[60] P.D. Cottle and O.N. Bignall, Phys. Rev. C **39**, 1158 (1989).
[61] Der-San Chuu, S.T. Hsieh, and H.C. Chiang, Phys. Rev. C **47**, 183 (1993).